ELSEVIER

Journal of Organometallic Chemistry 659 (2002) 125–132

Journal of Organometallic Chemistry

www.elsevier.com/locate/jorganchem

# Effects of counterions on intramolecular electron transfer in 1′,1‴-dinaphthylmethylbiferrocenium cation: structural, Mössbauer and EPR characteristics

Teng-Yuan Dong [a,*], Bor-Ruey Huang [a], Shie-Ming Peng [b], Gene-Hsiang Lee [b], Michael Y. Chiang [a]

[a] *Department of Chemistry, National Sun Yat-Sen University, Kaohsiung, Taiwan, ROC*
[b] *Department of Chemistry, National Taiwan University, Taipei, Taiwan, ROC*

Received 23 April 2002; received in revised form 21 May 2002; accepted 4 July 2002

**Abstract**

The effects of changing the counterion from $I_3^-$ to $BF_4^-$ and $PF_6^-$ anions upon the rate of intramolecular electron transfer in the mixed-valence 1′,1‴-dinaphthylmethylbiferrocenium cation are examined. The X-ray structural determinations of 1′,1‴-dinaphthylmethylbiferrocenium $BF_4^-$ and $PF_6^-$ salts are reported. The $^{57}$Fe Mössbauer and EPR results are also reported. We found that relatively minor perturbations caused by the crystallinity and counterions have pronounced effects on the magnitude of electron-transfer rate. 

*Keywords:* Mixed-valence 1′,1‴-dinaphthylmethylbiferrocenium; Biferrocenium; Metallocene; Electron transfer

## 1. Introduction

The rate of intramolecular electron transfer in mixed-valence biferrocenium cations can be sensitively controlled by environmental factors [1–19]. Studies of electron transfer in the series of mixed-valence biferrocenium compounds **1** (Scheme 1) revealed that the environment surrounding a cation is perhaps the most important factor in determining the rate of electron transfer. Compounds **1b** with short alkyl substituents ($n = 1$–4) give unusual temperature-dependent Mössbauer spectra [1–5]. At temperatures below 77 K they each show two Mössbauer doublets, one for the Fe(II) site and the other for the Fe(III) site (electron-transfer rate $< \sim 10^8$ s$^{-1}$). In each case, the two doublets move together with increasing the temperature, eventually, and become a single 'average-valence' doublet. It was suggested that the temperature dependence of the Mössbauer spectrum is due to the onset of lattice dynamics associated with the triiodide counterions and alkyl substituents.

In the case of mixed-valence cations **1b** with long alkyl substituents ($n > 4$), it has been known an even–odd character in the number of carbon atoms of the substituents in the relationship between the crystal structures and mixed-valenced state [20,21]. However, it seems difficult to separate the contribution of the symmetry of the cation and the packing effect in the crystal. The third strategy is the use of the derivatives attached to a planar substituent **1c** [22–24]. Mixed-valence 1′,1‴-dibenzylbiferrocenium triiodide (**1c**, $n = 1$) was reported [24] to have two distinct crystallographic phases which show that the electron-transfer rates are extremely sensitive to changes in crystal lattice. Two different crystalline morphologies (needle and plate-like) of 1′,1‴-dibenzylbiferrocenium triiodide were found. The needle crystal with space group $P\bar{1}$ has a Mössbauer spectrum characteristic of a valence-detrapped electronic structure down to a temperature of 25 K. The plate-like crystal with space group $P2_1/n$ shows a valence-trapped Mössbauer spectrum up to 300 K. However, because of the poor diffraction quality, a satisfactory refinement of the structure was not obtained. An

* Corresponding author. Fax: +7-525-3908
*E-mail address:* dty@mail.nsysu.edu.tw (T.-Y. Dong).

0022-328X/02/$ - see front matter 
PII: S0022-328X(02)01718-7

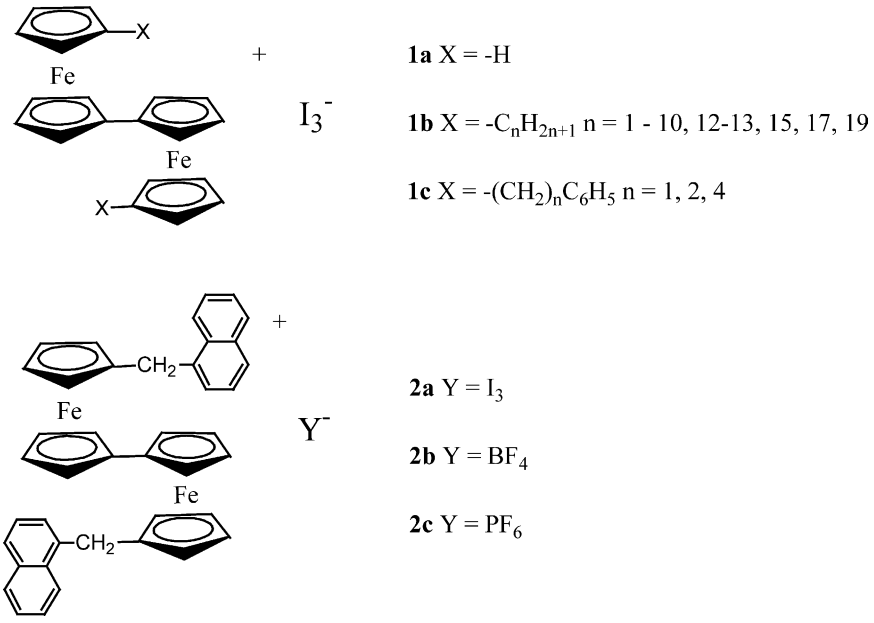


Scheme 1.

interesting finding is that there is a significant effect of changing the counterion from $I_3^-$ to $PF_6^-$, $AsF_6^-$, or $SbF_6^-$ upon the rate of intramolecular electron transfer in the 1′,1‴-dibenzylbiferrocenium cation.

Very recently, we found that 1′,1‴-dinaphthylmethylbiferrocenium triiodide (**2a**) has two distinct crystallographic phases and found that the electron-transfer rates are extremely sensitive to changes in crystal lattice [22,23]. Two different crystalline morphologies ($P\bar{1}$ and $P2_1/n$ phases) of **2a** were found. The cation with space group $P\bar{1}$ shows two doublets in the variable-temperature Mössbauer spectra at temperatures below 100 K. An increase in temperature causes the two doublets to move together, resulting in an average-valence doublet at 130 K, which is a characteristic of a valence-detrapped cation in which the electron-transfer rate exceeds $\sim 10^8$ $s^{-1}$. On the other hand, the cation with $P2_1/n$ phase exhibits a Mössbauer spectrum characteristic of a valence-trapped cation at 300 K. Obviously, the electron-transfer rate is quite sensitive to the environmental perturbation caused by different crystal packing arrangements.

The strategy of this study is the use of different counterions to show the close connection between the mixed-valence electronic state and the cation–anion interaction [25].

## 2. Results and discussion

### 2.1. Molecular structure of *2b*

Compound **2b** exhibits two distinguishable crystal morphologies; one polymorph crystallizes as needles, while the other crystallizes as plate-like crystals. Single-crystal structural determinations of both monoclinic morphologies with space group $P2_1/c$ were conducted at 298 K. Details of the X-ray crystal data collections and unit-cell parameters are given in Table 1, and selected bond distances and angles are given in Table 2. ORTEP-plots of two polymorphic crystals are given in Fig. 1. As given in Table 3, a direct comparison of the selected bond distances and angles is also made.

As shown in Fig. 1(a), the two metallocene moieties in the cation are not equivalent. The average Fe1–C distance (2.072(5) Å) and the Fe1–Cp distance (1.692

Table 1
Experimental and crystal data for the X-ray structures of **2b** and **2c**

| | **2b** | **2b** | **2c** |
|---|---|---|---|
| Formula | $C_{42}H_{34}BF_4Fe_2$ | $C_{42}H_{34}BF_4Fe_2$ | $C_{42}H_{34}PF_6Fe_2$ |
| Molecular weight | 737.20 | 737.20 | 795.39 |
| Crystal system | Monoclinic | Monoclinic | Monoclinic |
| Space group | $P2_1/c$ | $P2_1/c$ | $P2_1/c$ |
| $a$ (Å) | 9.267(2) | 16.427(3) | 9.028(5) |
| $b$ (Å) | 11.851(2) | 14.304(3) | 17.760(7) |
| $c$ (Å) | 30.581(4) | 14.261(4) | 22.427(4) |
| $\beta$ (°) | 95.94(2) | 95.99 | 99.49(2) |
| $V$ (Å$^3$) | 3340.2(11) | 3332.7(13) | 3547(2) |
| $Z$ | 4 | 4 | 4 |
| $D_{calc}$ (g cm$^{-3}$) | 1.466 | 1.469 | 1.489 |
| $\mu$ (mm$^{-1}$) | 0.922 | 0.924 | 0.924 |
| $\lambda$ (Å) | 0.71073 | 0.71073 | 0.71069 |
| $2\theta_{max}$ (°) | 50.00 | 50.00 | 52.2 |
| $R_1$ | 0.0544 | 0.0497 | 0.061 |
| $wR_2$ | 0.1583 | 0.1408 | |
| $wR$ | | | 0.078 |

$R_1 = \Sigma||F_o|-|F_c||/\Sigma|F_o|$; $wR_2 = [(\Sigma\ \omega(F_o^2-F_c^2)^2)/(\Sigma\ \omega F_o^2)^2]^{1/2}$; $wR = [\Sigma\ \omega(|F_o|-|F_c|)^2/\Sigma\ \omega F_o^2]^{1/2}$.

Table 2
Selective bond distances (Å) of **2b** and **2c**

| | **2b** [a] | **2b** [b] | **2c** |
|---|---|---|---|
| *Bond distances* | | | |
| Fe1–C1 | 2.109(5) | 2.146(4) | 2.035(6) |
| Fe1–C2 | 2.066(5) | 2.076(4) | 2.033(6) |
| Fe1–C3 | 2.046(5) | 2.040(5) | 2.038(6) |
| Fe1–C4 | 2.048(5) | 2.039(5) | 2.052(7) |
| Fe1–C5 | 2.079(5) | 2.083(4) | 2.029(7) |
| Fe1–C6 | 2.094(5) | 2.075(4) | 2.048(6) |
| Fe1–C7 | 2.065(5) | 2.058(5) | 2.039(7) |
| Fe1–C8 | 2.074(5) | 2.067(5) | 2.009(7) |
| Fe1–C9 | 2.061(5) | 2.105(5) | 2.018(7) |
| Fe1–C10 | 2.075(5) | 2.102(5) | 2.041(7) |
| Fe2–C11 | 2.082(4) | 2.036(4) | 2.128(6) |
| Fe2–C12 | 2.046(4) | 2.038(4) | 2.082(7) |
| Fe2–C13 | 2.046(5) | 2.036(5) | 2.061(6) |
| Fe2–C14 | 2.049(5) | 2.036(5) | 2.040(7) |
| Fe2–C15 | 2.047(4) | 2.037(4) | 2.076(7) |
| Fe2–C16 | 2.073(5) | 2.038(4) | 2.106(6) |
| Fe2–C17 | 2.047(5) | 2.045(4) | 2.068(7) |
| Fe2–C18 | 2.039(5) | 2.045(5) | 2.058(8) |
| Fe2–C19 | 2.039(5) | 2.035(5) | 2.082(8) |
| Fe2–C20 | 2.053(5) | 2.032(4) | 2.106(7) |
| B–F1 | 1.353(8) | 1.430(6) | |
| B–F2 | 1.335(7) | 1.238(7) | |
| B–F3 | 1.351(8) | 1.392(7) | |
| B–F4 | 1.331(8) | 1.325(6) | |
| P–F1 | | | 1.62(2) |
| P–F2 | | | 1.59(2) |
| P–F3 | | | 1.63(2) |
| P–F4 | | | 1.58(2) |
| P–F5 | | | 1.71(1) |
| P–F6 | | | 1.53(1) |

[a] Needle crystal.
[b] Plate-like crystal.

Å) indicate that this metallocene is in the Fe(III) oxidation state [26]. In contrast, the average Fe2–C distance (2.052(5) Å) and the average Fe2–Cp distance (1.660 Å) indicate that this metallocene is in the Fe(II) oxidation state [27]. The two Cp rings associated with Fe1 and Fe2 are not parallel, and the dihedral angles are 2.86 and 3.52°, respectively. Furthermore, the two Cp rings associated with Fe1 and Fe2 are not eclipsed but rotated relative to one another by 12.24 and 3.36°. It is important to find that the two metallocene units in the cation are twisted relative to each other. The two Cp rings in the fulvalenide bridge are not coplanar, and the dihedral angle between the Cp rings of the fulvalenide ligand is 7.83°. We believe that the degree of coplanarity between the two Cp rings in the fulvalenide bridge plays an important role in determining the magnitude of the electron-transfer rate. The structural determination of the needle crystal **2b** indicates that the cation is in the valence-trapped electronic state and this is consistent with our Mössbauer studies.

In plate-like crystal, the two metallocene moieties in the cation are also not equivalent as shown in Fig. 1(b).

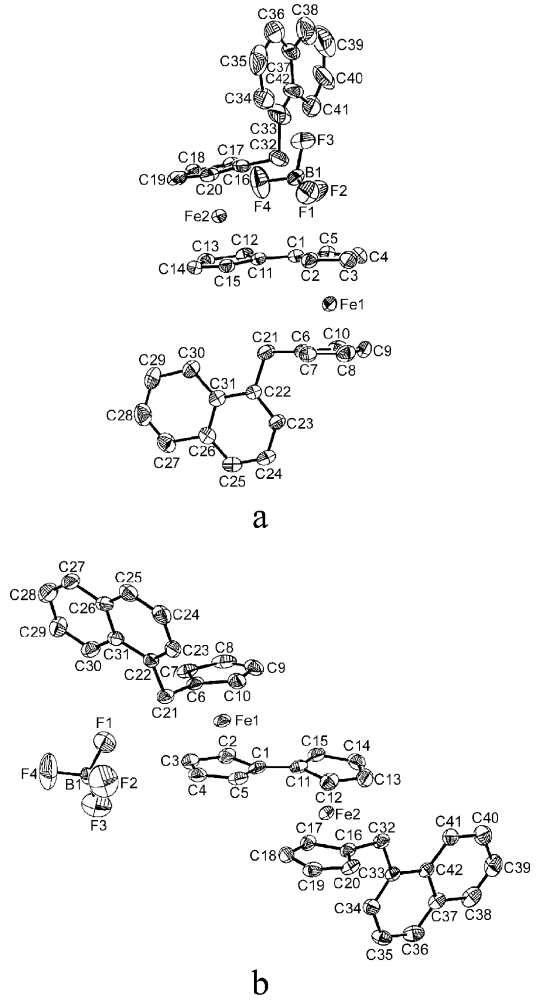


Fig. 1. Molecular view of **2b** with 30% thermal ellipsoids. Hydrogen atoms have been omitted for clarity. (a) ORTEP drawing of the needle crystal, and (b) ORTEP drawing of the plate-like crystal.

Table 3
Comparison of atomic distances and angles

| | **2b** [f] | **2b** [g] | **2c** |
|---|---|---|---|
| Fe(II)–C [a] | 2.052(5) | 2.038(5) | 2.036(6) |
| Fe(III)–C [a] | 2.072(5) | 2.079(5) | 2.070(6) |
| Fe(II)–Cp [b] | 1.661 | 1.645 | 1.645 |
| Fe(III)–Cp [b] | 1.692 | 1.697 | 1.699 |
| Stag-Fe(II) [c] | 3.36 | 6.6 | 8.93 |
| Stag-Fe(III) [c] | 12.24 | 0.4 | 14.69 |
| Dihe-Fe(II) [d] | 3.52 | 2.10 | 3.15 |
| Dihe-Fe(III) [d] | 2.86 | 7.98 | 3.58 |
| Dihe-ful [e] | 7.83 | 13.10 | 4.28 |

[a] Average Fe–C distance.
[b] The average distance between the Fe atom and the Cp ring.
[c] Stagger angle between the two Cp rings associated with the corresponding Fe atom.
[d] Dihedral angle between the two Cp rings associated with the corresponding Fe atom.
[e] Dihedral angle between the two Cp rings in the fulvalenide ligand.
[f] Needle crystal.
[g] Plate-like crystal.

The average Fe1–C distance and the Fe1–Cp distance indicate that this metallocene is in the Fe(III) oxidation state [26]. Inspection of the Fe2–C distance and the Fe2–Cp distance shows that this metallocene is in the Fe(II) oxidation state [27]. The two Cp rings in the fulvalenide bridge are also not coplanar, and the dihedral angle between the Cp rings of the fulvalenide ligand is 13.10°.

A comparison of structural features between the two different crystallographic phases of **2b** is interesting. The naphthylmethyl substituent on the Cp ring is situated differently. The two nonequivalent naphthylmethyl substituents in the needle crystal show a cisoid conformation relative to the fulvalenide ligand, and this is similar to other dialkyl mixed-valence triiodide salts [1–5]. In the case of plate-like crystal, the two nonequivalent naphthylmethyl substituents show a transoid conformation relative to the fulvalenide ligand. Consequently, the packing arrangement of the needle crystal of **2b** is different from that of the plate-like crystal.

### 2.2. Molecular structure of *2c*

Details of the X-ray crystal data collection and the unit-cell parameters are also given in Table 1, and the selected bond distances are given in Table 2. The molecular structure of **2c** is shown in Fig. 2. A comparison of the selected distances and angles between **2b** and **2c** is made as shown in Table 3.

Compound **2c** has the usual conformation seen in other dialkyl mixed-valence biferrocenium triiodide salts [1–5]. The two metallocene moieties in the cation are not equivalent. The average Fe1–C distance (2.036(6) Å) and the Fe1–Cp distance (1.645 Å) indicate that this metallocene is in the Fe(II) oxidation state [27]. The average Fe2–C distance (2.070(6) Å) and the average Fe2–Cp distance (1.699 Å) indicate that this metallocene is in the Fe(III) oxidation state [26]. The two Cp rings associated with Fe1 and Fe2 are not quite parallel, and the dihedral angles are 3.15 and 3.58°, respectively. The two Cp rings associated with Fe1 and Fe2 are not eclipsed, with average staggering angles of 8.93 and 14.69°, respectively. The two Cp rings in the fulvalenide bridge are nearly coplanar, and the dihedral angle between the Cp rings of the fulvalenide ligand is 4.28°. The X-ray structural determination of **2c** also indicates the cation in **2c** has a valence-trapped electronic structure.

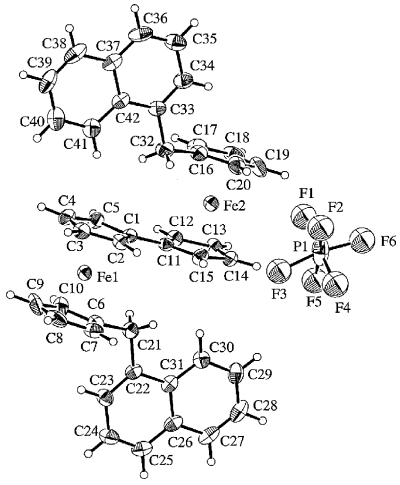


Fig. 2. Molecular view of **2c** with 30% thermal ellipsoids. Hydrogen atoms have been omitted for clarity.

### 2.3. $^{57}$Fe Mössbauer characteristics

We examined the microcrystalline sample of **2b**, formed by adding an ether solution of 0.1 M $HBF_4$ to a benzene solution of neutral biferrocene and stoichiometric amount of *p*-benzoquinone. The variable-temperature $^{57}$Fe Mössbauer spectra are shown in Fig. 3. The various absorption peaks were fitted to the Lorentzian lines. The resulting fitting parameters are collected in Table 4. The prominent features in the 300 and 80 K $^{57}$Fe Mössbauer spectra of the microcrystalline sample of **2b** are two doublets, one with a $\Delta E_Q \approx 2.2$ mm $s^{-1}$ (Fe(II) metallocene) and the other with a $\Delta E_Q \approx 0.4$ mm $s^{-1}$ (Fe(III) metallocene). The area ratio of the Fe(II) doublet to the Fe(III) doublet is nearly equal to 1. This pattern of two doublets is what is expected for a mixed-valence biferrocenium cation which is valence-trapped on the Mössbauer time-scale.

Two different crystalline morphologies of **2b** were also examined with variable-temperature Mössbauer spectroscopy. Similar observations that have been made for the microcrystalline sample of **2b** have also been seen for the two crystalline morphologies of **2b**. As shown in Table 4, two doublets can be seen in each case, characteristic of a valence-trapped electronic structure.

On the other hand, the microcrystalline sample of **2c** exhibits an interesting Mössbauer behavior. An increase

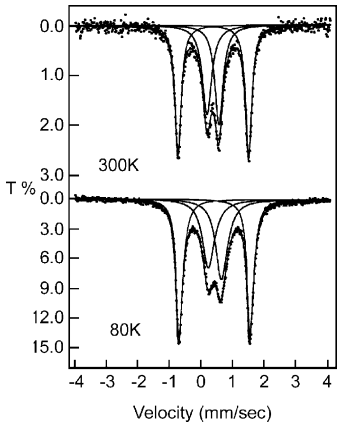


Fig. 3. Variable-temperature $^{57}$Fe Mössbauer spectra of the microcrystalline sample of **2b**.

Table 4
$^{57}$Fe Mössbauer least-squares-fitting parameters

| Compound | $T$ (K) | $\Delta E_Q$ [a] | $\delta$ [b] | $\Gamma$ [c] | Area ratio [d] |
|---|---|---|---|---|---|
| **2a** ($P\bar{1}$) [e] | 300 | 1.120 | 0.451 | 0.441, 0.427 | |
| | 110 | 1.516, 0.902 | 0.516, 0.523 | 0.511, 0.456, 0.450, 0.459 | 1.00 |
| | 80 | 1.610, 0.818 | 0.516, 0.528 | 0.511, 0.502, 0.543, 0.498 | 1.00 |
| **2a** ($P2_1/n$) [e] | 300 | 2.087, 0.407 | 0.441, 0.430 | 0.267, 0.251, 0.285, 0.281 | 1.00 |
| **2b** [f] | 300 | 2.225, 0.373 | 0.432, 0.425 | 0.246, 0.237, 0.356, 0.312 | 0.98 |
| | 80 | 2.211, 0.412 | 0.515, 0.520 | 0.254, 0.251, 0.466, 0.446 | 1.02 |
| **2b** [g] | 300 | 2.141, 0.353 | 0.420, 0.405 | 0.314, 0.289, 0.353, 0.324 | 0.99 |
| | 80 | 2.322, 0.414 | 0.535, 0.526 | 0.326, 0.320, 0.695, 0.643 | 1.00 |
| **2b** [h] | 300 | 2.191, 0.351 | 0.431, 0.421 | 0.261, 0.259, 0.312, 0.303 | 1.01 |
| | 80 | 2.211, 0.400 | 0.515, 0.523 | 0.244, 0.242, 0.534, 0.442 | 1.00 |
| **2c** [f] | 300 | 1.550, 0.813 | 0.424, 0.432 | 0.713, 0.706, 0.571, 0.552 | 1.00 |
| | 250 | 2.3105, 0.8762 | 0.561, 0.572 | 0.611, 0.610, 0.568, 0.563 | 1.00 |
| | 80 | 2.054, 0.532 | 0.510, 0.515 | 0.357, 0.354, 0.501, 0.483 | 1.00 |
| **2c** [i] | 300 | 2.214, 0.511 | 0.431, 0.508 | 0.252, 0.245, 0.414, 0.483 | 0.39 |
| | 80 | 2.230, 0.484 | 0.518, 0.521 | 0.260, 0.276, 0.472, 0.467 | 0.85 |

[a] Quadrupole-splitting in mm s$^{-1}$.
[b] Isomer shift referenced to iron foil in mm s$^{-1}$.
[c] Full-width at half-height taken from the least-squares-fitting program. The width for the line at more positive velocity is listed first for each doublet.
[d] The area ratio of the Fe(II) doublet over the Fe(III) doublet.
[e] From ref. [23].
[f] Microcrystalline sample.
[g] Needle sample.
[h] Plate-like crystalline sample.
[i] Crystalline sample.

of temperature causes the two doublets to move together, $\Delta E_Q = 1.550$ and 0.813 mm s$^{-1}$ at 300 K. The variable-temperature Mössbauer spectra of the microcrystalline sample of **2c** are shown in Fig. 4.

The crystalline sample gives a Mössbauer spectrum at 300 K that shows two doublets ($\Delta E_Q = 2.214$ and 0.511 mm s$^{-1}$). The variable-temperature Mössbauer spectra obtained for a crystalline sample are shown in Fig. 5. In the crystalline sample of **2c**, as the temperature is increased, the two doublets seen in the low temperature Mössbauer spectrum do not move together to coalesce into a broaden doublet at high temperature. Obviously, the intramolecular electron transfer is quite sensitive to the environmental perturbations caused by different crystallinity and counterions.

Furthermore, it is curious to find that the area ratio between the Fe(II) doublet and the Fe(III) doublet in the 300 K $^{57}$Fe Mössbauer spectrum of the microcrystalline and the crystalline samples of **2c** is not equal to 1.

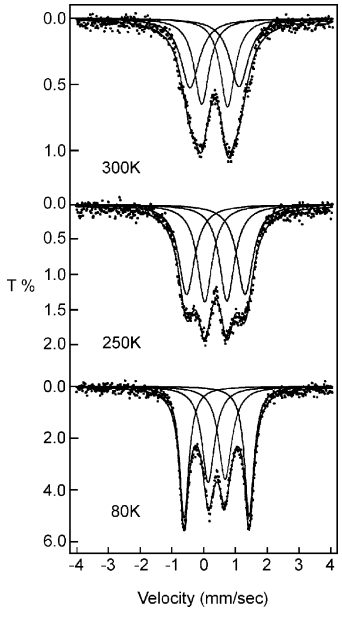


Fig. 4. Variable-temperature $^{57}$Fe Mössbauer spectra of the microcrystalline sample of **2c**.

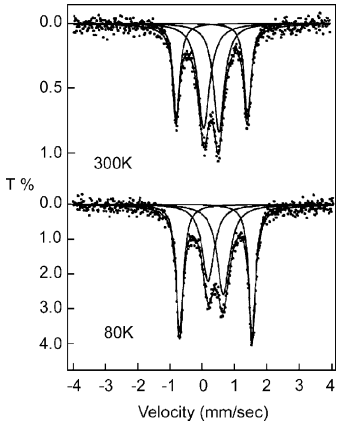


Fig. 5. Variable-temperature $^{57}$Fe Mössbauer spectra of the crystalline sample of **2c**.

However, the area ratio of the Fe(II) doublet over the Fe(III) doublet in the 80 K Mössbauer spectra of the microcrystalline and crystalline samples is nearly equal to 1. The ratio changes from 0.9–1.1 to 0.4–0.5 as the temperature is changed from 80 to 300 K. This observation can be interpreted in terms of a different temperature dependence of the Mössbauer recoil energy fraction between the Fe(II) and Fe(III) sites.

### 2.4. Electron paramagnetic resonance

X-band EPR spectra were run for the samples of **2b** and **2c** at 77 K. The 77 K spectra for **2b** and **2c** are clearly axial-type spectra [24], and the $g$-values evaluated from these spectra and other related EPR spectra are collected in Table 5. In the case of **2b**, the $g$-values are not sensitive with the crystallinity of sample. However, the dependence of the crystallinity of sample on the $g$-values can be observed in **2c**. In the case of the microcrystalline sample of **2c**, the value of the $g$-tensor anisotropy ($\Delta g$) is considerably reduced. This is consistent with our Mössbauer studies. As shown in Table 5, there is a correlation between the values of $\Delta g$ and $\Delta\Delta E_Q$: the smaller $\Delta g$ value, the smaller $\Delta\Delta E_Q$ value (or the faster rate of electron transfer). Of course, the reduced $\Delta g$ value is a reflection of an admixture of the Fe(II) and Fe(III) electronic configurations.

## 3. Conclusion

An amazing change in the Mössbauer characteristics results when the $I_3^-$ anion of **2a** is replaced by the $BF_4^-$ anion and $PF_6^-$ anion. Samples of **2b** and crystalline sample of **2c** is localized at 300 K. The change from $I_3^-$ (**2a** with $P\bar{1}$ phase) to $BF_4^-$ lead to a change of $\sim$170 K in the temperature at which the mixed-valence 1′,1‴-dinaphthylmethylbiferrocenium cation transfers electron slower than the Mössbauer time scale.

In the case of **2c**, the crystallinity of sample has pronounced effects on the electronic structure. The possibility of various kinds of conformational arrangements caused by different counterions and the dependence of the crystallinity of sample on electronic structure clearly indicate that the environment about the mixed-valence cation plays an important role in determining the magnitude of intramolecular electron-transfer rate.

Table 5
EPR data of **2** and other related compounds

| Compound [a] | $T$ (K) | $g_\parallel$ | $g_\perp$ | $\Delta g$ [b] |
|---|---|---|---|---|
| **1a** [c] | 4.2 | 3.58 | 1.72 | 1.86 |
| **1b** ($n=4$) [c] | 4.2 | 2.98 | 1.92 | 1.06 |
| **1c** ($n=1$) [d] | 4.2 | 3.02 | 2.01, 1.89 | 1.07 |
| **2a** ($P\bar{1}$ phase) [e] | 77 | 3.16 | 1.91 | 1.25 |
| **2a** ($P2_1/n$ phase) [e] | 77 | 3.67 | 2.01 | 1.66 |
| **2b** [f] | 77 | 3.36 | 1.83 | 1.53 |
| **2b** [g] | 77 | 3.35 | 1.85 | 1.50 |
| **2b** [h] | 77 | 3.31 | 1.82 | 1.49 |
| **2c** [f] | 77 | 3.25 | 1.98 | 1.27 |
| **2c** [i] | 77 | 3.36 | 1.83 | 1.53 |

[a] Powder samples.
[b] $\Delta g = g_\parallel - g_\perp$.
[c] From ref. [2].
[d] From ref. [24].
[e] From ref. [23].
[f] Microcrystalline sample.
[g] Needle crystalline sample.
[h] Plate-like crystalline sample.
[i] Crystalline sample.

## 4. Experimental

### 4.1. General information

All manipulations involving air-sensitive materials were carried out by using standard Schlenk techniques under an atmosphere of $N_2$. Chromatography was performed on neutral alumina (Merck, activity II). Sample of 1′,1‴-dinaphthylmethylbiferrocene was prepared according to the literature procedure [23].

### 4.2. Mixed-valence compounds *2b* and *2c*

Microcrystalline sample of **2** was prepared by adding an ether solution of 0.1 M $HBF_4$ or $HPF_6$ to a benzene solution of 1′,1‴-dinaphthylmethylbiferrocene containing a stoichiometric amount of $p$-benzoquinone. The resulting dark crystals were filtered and washed repeatedly with benzene–ether (3:1). Recrystallization was carried out from $CH_2Cl_2$–hexane as solvent. Anal. Calc. for **2b** ($C_{42}H_{34}BF_4Fe_2$): C, 68.43; H, 4.65. Found: C, 68.45; H, 4.64%. Anal. Calc. for **2c** ($C_{42}H_{34}PF_6Fe_2$): C, 63.41; H, 4.31. Found: C, 63.41; H, 4.42%.

Crystalline sample can be prepared by slowly diffusing hexane into a $CH_2Cl_2$ solution containing the corresponding biferrocenium salt. In the case of **2b**, two distinct crystalline morphologies were apparent: needle and plate-like crystals. The crystal morphologies were separated into two samples.

### 4.3. Physical methods

$^{57}$Fe Mössbauer measurements were made on a constant-velocity instrument which has been previously described [18]. The absolute temperature accuracy is estimated to be $\pm$5 K, while the relative precision is $\pm$ 0.5 K. Computer fittings of the $^{57}$Fe Mössbauer data to Lorentzian lines were carried out with a modified version of a previously reported program [28]. Velocity calibrations were made using a 99.99% iron foil.

Electron paramagnetic resonance data (X-band) was collected with a Bruker ER200D-SRC spectrometer. The magnetic field was calibrated with a Bruker ER035M NMR gaussmeter. DPPH was used to gauge the microwave frequency. A direct-immersion dewar, which was inserted into the cavity, was use to obtain 77 K data.

### 4.4. Structural determination of needle crystal of **2b**

A dark crystal ($0.75 \times 0.37 \times 0.17$ mm), which was grown when a layer of hexane was allowed to slowly diffuse into a $CH_2Cl_2$ solution of **2b**, was used for data collection at 298 K. Cell dimensions (obtained from 25 reflections) and space group data were obtained by standard methods on Siemens SMART CCD diffractometer. The $\theta-2\theta$ scan technique was used to record the intensities for all reflections for which $1.84 < \theta < 25.00^\circ$. Absorption corrections were made with empirical $\Psi$-rotation. The X-ray crystal data are summarized in Table 1.

A three-dimensional Patterson synthesis was used to determine the heavy-atom positions, which phased the data sufficiently well to permit location of the remaining non-hydrogen atoms from Fourier synthesis. All non-hydrogen atoms were refined anisotropically. During the final cycles of refinement, fixed hydrogen contributions with C–H bond lengths fixed were applied. The selected bond distances are given in Table 2. The final positional parameters for all atoms, thermal parameters, and complete table of bond distances and angles are given as supplementary materials.

### 4.5. Structural determination of plate-like crystal of **2b**

Data were collected to a $2\theta$-value of $50.00^\circ$ for a dark crystal ($0.50 \times 0.50 \times 0.35$ mm). Details of data collection and unit cell parameters are given in Table 1. Structure refinement was carried out in the same manner as described for needle crystal of **2b**.

### 4.6. Structural determination of **2c**

A dark crystal ($0.30 \times 0.62 \times 0.76$ mm), which was obtained when a layer of hexane was allowed to slowly diffuse into a $CH_2Cl_2$ solution of **2c**, was used for data collection at 298 K on a Rigaku AFC7S diffractometer. Details of data collection and unit cell parameters are also given in Table 1. Structure refinement was carried out in the same manner as described for needle crystal of **2b**.

## 5. Supplementary material

Tables of atomic, positional and thermal parameters, bond angles and distances. Crystallographic data for the structural analysis has been deposited with Cambridge Crystallographic Data Centre, CCDC numbers 151980, 182904, and 182903 for needle crystal of **2b**, plate-like crystal of **2b**, and **2c**, respectively. Copies of this information maybe obtained free of charge from The Director, CCDC, 12 Union Road, Cambridge CB2 1EZ, UK (Fax: +44-1223-336033; e-mail: deposit@ccdc.cam.ac.uk or www: http://www.ccdc.cam.ac.uk).

## Acknowledgements

Acknowledgments are made to the National Science Council (NSC90-2113-M-110-014), Taiwan, ROC, and Department of Chemistry at Sun Yat-Sen University.

## References

[1] D.N. Hendrickson, S.M. Oh, T.-Y. Dong, T. Kambara, M.J. Cohn, M.F. Moore, Comments Inorg. Chem. 4 (1985) 329.
[2] T.-Y. Dong, D.N. Hendrickson, K. Iwai, M.J. Cohn, S.J. Geib, A.L. Rheingold, H. Sano, I. Motoyama, S. Nakashima, J. Am. Chem. Soc. 107 (1985) 7996.
[3] T.-Y. Dong, D.N. Hendrickson, C.G. Pierpont, M.F. Moore, J. Am. Chem. Soc. 108 (1986) 963.
[4] S. Iijima, R. Saida, I. Motoyama, H. Sano, Bull. Chem. Soc. Jpn. 54 (1981) 1375.
[5] (a) S. Nakashima, M. Katada, I. Motoyama, H. Sano, Bull. Chem. Soc. Jpn. 60 (1987) 2253;
(b) S. Nakashima, M. Katada, I. Motoyama, H. Sano, Bull. Chem. Soc. Jpn. 59 (1986) 2923;
(c) S. Nakashima, Y. Masuda, I. Motoyama, H. Sano, Bull. Chem. Soc. Jpn. 60 (1987) 1673;
(d) S. Nakashima, T. Oka, T. Okuda, M. Watanabe, Inorg. Chem. 38 (1999) 4005.
[6] M. Kai, M. Katada, H. Sano, Chem. Lett. (1988) 1523.
[7] T.-Y. Dong, C.C. Schei, T.L. Hsu, S.L. Lee, S.J. Li, Inorg. Chem. 30 (1991) 2457.
[8] T.-Y. Dong, C.Y. Chou, J. Chem. Soc. Chem. Commun. (1990) 1332.
[9] T.-Y. Dong, C.C. Schei, M.Y. Hwang, T.Y. Lee, S.K. Yeh, Y.S. Wen, Organometallics 11 (1992) 573.
[10] R.J. Webb, S.J. Geib, D.L. Staley, A.L. Rheingold, D.N. Hendrickson, J. Am. Chem. Soc. 112 (1990) 5031.
[11] R.J. Webb, A.L. Rheingold, S.J. Geib, D.L. Staley, D.N. Hendrickson, Angew. Chem. Int. Ed. Engl. 28 (1989) 1388.
[12] T.-Y. Dong, T. Kambara, D.N. Hendrickson, J. Am. Chem. Soc. 108 (1986) 5857.
[13] T.-Y. Dong, T. Kambara, D.N. Hendrickson, J. Am. Chem. Soc. 108 (1986) 4423.
[14] H.G. Gang, S.J. Geib, Y. Kaneko, M. Nakano, M. Sorai, A.L. Rheingold, B. Montez, D.N. Hendrickson, J. Am. Chem. Soc. 111 (1989) 173.
[15] Y. Kaneko, M. Nakano, M. Sorai, H.G. Jang, D.N. Hendrickson, J. Am. Chem. Soc. 28 (1989) 1067.
[16] T.-Y. Dong, T.Y. Lee, M.H. Lin, J. Organomet. Chem. 427 (1992) 101.

[17] T.-Y. Dong, C.K. Chang, C.H. Huang, Y.S. Wen, S.L. Lee, J.A. Chen, W.Y. Yeh, A. Yeh, J. Chem. Soc. Chem. Commun. (1992) 526.
[18] T.-Y. Dong, C.H. Huang, C.K. Chang, Y.S. Wen, S.L. Lee, J.A. Chen, W.Y. Yeh, A. Yeh, J. Am. Chem. Soc. 115 (1993) 6357.
[19] T.-Y. Dong, S.H. Lee, C.K. Chang, H.M. Lin, K.J. Lin, Organometallics 16 (1997) 2773.
[20] S. Nakashima, S. Nakszaki, H. Sakai, M. Watanabe, I. Motoyama, M. Sato, Inorg. Chem. 37 (1998) 1959.
[21] S. Nakashima, Y. Ueki, H. Sakai, J. Chem. Soc. Dalton Trans. (1995) 513.
[22] (a) T.-Y. Dong, X.Q. Lai, Z.W. Lin, K.J. Lin, Angew. Chem. Int. Ed. Engl. 36 (1997) 2002;
(b) S. Nakashima, A. Hori, H. Saskai, M. Watanabe, I. Motoyama, J. Organomet. Chem. 542 (1997) 271.
[23] T.-Y. Dong, P.H. Ho, X.Q. Lai, Z.W. Lin, K.J. Lin, Organometallics 19 (2000) 1096.
[24] R.J. Webb, T.-Y. Dong, C.G. Pierpont, S.R. Boone, R.K. Chadha, D.N. Hendrickson, J. Am. Chem. Soc. 113 (1991) 4806.
[25] T.-Y. Dong, T.J. Lee, B.R. Huang, S.M. Peng, G.H. Lee, Inorg. Chem. Commun. 4 (2001) 82.
[26] N.J. Mammano, A. Zalkin, A. Landers, A.L. Rheingold, Inorg. Chem. 16 (1977) 297.
[27] P. Seiler, J.D. Dunitz, Acta Crystallogr. Sect. B 35 (1979) 1068.
[28] J.F. Lee, M.D. Lee, P.K. Tseng, Chemistry 45 (1987) 50 (in Chinese).